Journal of Power Sources 205 (2012) 307–317

Contents lists available at SciVerse ScienceDirect

Journal of Power Sources

journal homepage: www.elsevier.com/locate/jpowsour

Joint strength of a solid oxide fuel cell glass–ceramic sealant with metallic interconnect

Chih-Kuang Lin[a,*], Jun-Yu Chen[a], Jie-Wun Tian[a], Lieh-Kwang Chiang[b], Si-Han Wu[b]

[a] Department of Mechanical Engineering, National Central University, Jhong-Li 32001, Taiwan
[b] Nuclear Fuel & Material Division, Institute of Nuclear Energy Research, Lung-Tan 32546, Taiwan

ARTICLE INFO

Article history:
Received 27 October 2011
Received in revised form
20 December 2011
Accepted 1 January 2012
Available online 10 January 2012

Keywords:
Planar solid oxide fuel cell
Glass–ceramic sealant
Metallic interconnect
Joint strength
Pre-oxidation treatment
Thermal aging

ABSTRACT

The aim of this study is to investigate the joint strength between a newly developed glass–ceramic sealant (GC-9) and metallic interconnect (Crofer 22 H) for planar solid oxide fuel cells (pSOFCs). The joint strength is evaluated at room temperature and 800 °C under shear and tensile loading using two types of sandwich specimen. Effects of number of initial sealant-spreading side, pre-oxidation of metallic interconnect, and thermal aging in air on the joint strength are studied. Regardless of testing temperature and loading mode, the joint strength of specimens initially with two sides of glass–ceramic sealant is greater than that of single-sided ones. A pre-oxidation treatment of the metal coupon at 900 °C for 2 h or 20 h does not generate a beneficial effect on the shear and tensile joint strength for all the given testing conditions. Compared to the shear strength of unaged joint specimens, a reduction of 17–19% in shear joint strength at 800 °C is observed for variously aged ones.

1. Introduction

Solid oxide fuel cells (SOFCs) have the highest efficiencies among the fuel cells developed as they utilize solid ceramics as the electrolyte and electrode and operate at high temperatures. In recent development of SOFCs, planar SOFCs (pSOFCs) have attracted more attention as they are easier to fabricate, operate at a lower temperature (below 800 °C), and offer a higher power density over the tubular ones. In practical applications of pSOFCs, unit cells are integrated by bipolar interconnects into a multi-cell stack to generate a high voltage and power. Therefore, interconnects play a very important role in structural and electrical connection of unit cells. During the stacking process and operation, hermetic sealants are needed to maintain gas tight between components in SOFCs. Sealants for SOFCs must have necessary adherence, mechanical integrity, chemical stability and compatibility, electric insulation, and thermal expansion match at operating temperature. The high-temperature operation, however, gives rise to significant thermal stresses due to mismatch of coefficient of thermal expansion (CTE) between components and temperature gradients in the SOFC system [1,2].

When a rigid type of sealing is applied to pSOFCs, joining glass–ceramic sealants to metallic interconnects is very common. During cyclic operation of pSOFCs, generation of thermal stresses is inevitable leading the seals to be subjected to tensile and shear stresses [1,2]. Once the stresses exceed the corresponding strength of the joint between a glass–ceramic sealant and metallic interconnect, failure of the sealing may lead to gas leakage and degradation of cell performance. For this reason, it is necessary to investigate the mechanical properties of such a joint for assessing the structural reliability of a pSOFC stack. The mechanical properties of a joint do not belong to that of a single material while they are interfacial properties between two materials. Any interaction between the glass–ceramic and metal may influence the mechanical properties of the joint. Although many studies, e.g. [3–9], have recently investigated the bonding and chemical interaction of glass–ceramic sealants with metallic interconnects, little literature is related to the mechanical properties of such joints in pSOFCs. Only a limited number of studies [10–13] have been focused on this subject which is important to advance the development of SOFC technologies.

In the study of Smeacetto et al. [10], bonding strength between a glass–ceramic sealant (SiO_2–Al_2O_3–CaO–Na_2O, SACN) and two Cr-containing metallic interconnects (Crofer 22 APU and AISI 430) was evaluated under tensile loading at room temperature, but no quantitative data of mechanical strength were reported. It was found that fracture of the Crofer 22 APU/SACN/Crofer 22 APU joint specimens always occurred within the glass–ceramic layer and never at the interfaces in the joint [10]. In order to obtain a good adhesion between the AISI 430 steel and SACN glass–ceramic, a pre-oxidation treatment of the metal is essential [10]. Chou et al. [11,12] investigated the tensile joint strength of a (SrO,CaO)–Y_2O_3–B_2O_3–SiO_2

* Corresponding author. Tel.: +886 3 426 7340; fax: +886 3 425 4501.
E-mail address: t330014@cc.ncu.edu.tw (C.-K. Lin).

0378-7753/$ – see front matter © 2012 Elsevier B.V. All rights reserved.
doi:10.1016/j.jpowsour.2012.01.048

glass (YSO75) with a Crofer 22 APU interconnect at room temperature and found that the bonding behavior of the joint was intensely dependent on the nature of the metal surface. The joint strength of the YSO75 glass with Crofer 22 APU at room temperature was degraded if the thickness of oxide scale on Crofer 22 APU was greater than 1–2 μm while oxide scales thinner than 0.5 μm had no influence on the joint strength [11]. In other words, the applied pre-oxidation treatments of Crofer 22 APU had no positive effect on the Crofer 22 APU/YSO75/Crofer 22 APU joint strength [11]. The results in Refs. [10,11] show a different trend in terms of pre-oxidation effect. Accordingly, further research is needed to investigate such an issue.

Stephens et al. [13] studied the interfacial strength between a G18 glass–ceramic and Crofer 22 APU substrate and found that the joint strength under tensile and shear loading was decreased with an increase in temperature from 25 to 800 °C. Failure occurring either through the glass layer or at the glass–metal interface was found in tensile tests while in shear tests only interfacial failure took place for the G18/Crofer 22 APU joints [13]. Pre-oxidation effect was not considered in that study [13]. As new glass/glass–ceramic sealants and metallic interconnects have recently been developed for pSOFCs, more studies on the joint strength between glass/glass–ceramic sealants and metallic interconnects at both room temperature and operating temperature are needed to provide more comprehensive information for design of a reliable pSOFC stack. As part of a series of studies [14–18] on the mechanical properties of glass–ceramic sealants and metallic interconnects for pSOFCs, the aim of this study is to investigate the tensile and shear joint strength between a newly developed glass–ceramic sealant (GC-9) and metallic interconnect (Crofer 22 H) for pSOFC applications. In particular, effects of number of initial sealant-spreading side, pre-oxidation, and thermal aging on the bonding strength are evaluated at both room temperature and 800 °C.

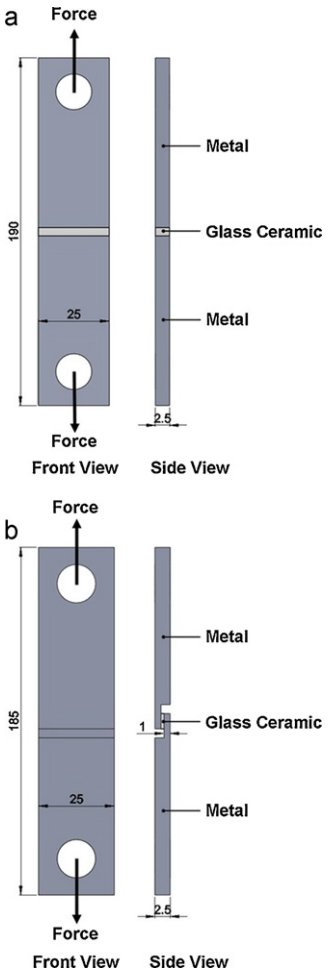

Fig. 1. Scheme of two types of joint specimen: (a) tensile specimen and (b) shear specimen (dimensions: mm).

2. Experimental procedures

2.1. Materials and specimens

Fig. 1(a) and (b) shows two types of joint specimen for tensile and shear tests, respectively. The glass–ceramic sealant, designated as GC-9, used to join the two metallic coupons is a novel $BaO–B_2O_3–Al_2O_3–SiO_2$ glass which has recently been developed at the Institute of Nuclear Energy Research (INER) for pSOFCs [19–23]. Chemical composition of the GC-9 glass includes 0–40 mol% BaO, 0–15 mol% B_2O_3, 0–10 mol% Al_2O_3, 0–40 mol% SiO_2, 0–15 mol% CaO, 0–15 mol% La_2O_3, and 0–5 mol% ZrO_2. The GC-9 glass sealant shows good thermal properties, chemical compatibility and stability, and hermetic properties for use in pSOFCs [19–23]. The glass transition temperature (T_g) and softening temperature (T_s) of the GC-9 glass are at 668 °C and 745 °C, respectively [16]. High-temperature mechanical properties of the GC-9 glass–ceramic in both bulk and sintered forms have been well studied [14–16].

The metallic coupons of the joint specimens were made of a newly developed commercial ferritic stainless steel, Crofer 22 H (ThyssenKrupp VDM GmbH, Germany), which is a heat-resistant alloy developed for pSOFC interconnects. The chemical composition of Crofer 22 H alloy in wt% includes 22.93 Cr, 1.94 W, 0.51 Nb, 0.43 Mn, 0.21 Si, 0.08 La, 0.07 Ti, 0.02 Cu, 0.02 Al, 0.014 P, 0.007 C, <0.002 S, and balance of Fe. With the additions of 0.51 wt% of Nb and 1.94 wt% of W, Crofer 22 H alloy shows better electrical conductivity, oxidation resistance, tensile strength, and creep resistance for pSOFC applications, as compared to the previously developed Crofer 22 APU steel [17,18,24,25]. The as-received Crofer 22 H plates were cut into slices with dimensions of 95 mm (length) × 25 mm (width) × 2.5 mm (thickness) to make the joint specimens. A pin hole was drilled in each steel slice for applying pin loading. In order to minimize the bending and twisting effects during mechanical testing, the force was applied by means of pin loading. For shear specimens, an edge of each steel slice was milled from the original thickness of 2.5 mm to 1 mm with an area of 8 mm × 25 mm.

After machining the steel slices, GC-9 glass paste was spread on the joining region of each steel coupon to make a half specimen. The nominal joining areas are of 25 mm × 2.5 mm and 25 mm × 6 mm for tensile and shear specimens, respectively. The glass paste was made of a mixture of GC-9 glass powders dispersed in ethanol. The half specimens were dried in furnace at 70 °C after spreading the glass paste. A single-sided joint specimen (designated as HT900S) was assembled by placing a half specimen on another plain steel slice to form a metal/glass–ceramic/metal sandwich specimen through appropriate heat treatments. For studying the effect of number of initial spreading side of glass paste on the joint strength, a half specimen was alternatively placed on another half specimen to form a double-sided joint specimen (designated as HT900D) through the same joining heat treatments. In order to make both sides of the sandwich joint specimen flat to avoid any bending effect on the mechanical test, a special fixture was made and used to hold the specimen during the joining heat treatments. Each preliminarily assembled specimen together with the holding fixture was then heated to 500 °C and held for 1 h followed by another heating step to 900 °C with a hold time of 4 h to complete the joining process. The heating rate at each heating step in the given joining process is 5 °C min^{-1}. After the joining process is completed,

the thickness of glass–ceramic sealant is of 0.5 mm for both single-sided and double-sided shear joint specimens. The glass–ceramic sealant in the double-sided and single-sided tensile joint specimens has a thickness of 0.44 mm and 0.22 mm, respectively. For investigating the effect of oxide layer on the bonding strength, some steel slices were pre-oxidized at 900 °C for 2 h or 20 h before spreading the glass–ceramic sealant. To study the effect of thermal aging on the joint strength, some joint specimens were aged in air at 800 °C for 250, 500, or 1000 h after the joining process.

2.2. Mechanical testing

For determining mechanical properties of the joints at room temperature and 800 °C, the specimens were tested under uni-axial loading on a commercial closed-loop servo-hydraulic test machine attached with a furnace. For the high-temperature tests, joint specimens were heated to 800 °C with a rate of 5 °C min^{-1} and held for 15 min to reach thermal equilibrium before applying mechanical loads. The mechanical tests were conducted under displacement control with a stroke rate of 0.5 mm min^{-1}. For each investigated condition, 5–7 specimens were repeatedly tested and the average strength was determined.

2.3. Microstructural analysis

After mechanical testing, fracture surfaces of each specimen were examined with an optical microscope to determine the true joining area for calculating the nominal tensile or shear stress. In order to characterize the interfaces in the joint specimens, some samples were cut along the longitudinal direction to observe the cross sections. These cross sections were finely polished to optical finish. Scanning electron microscopy (SEM) was applied to examine the interfacial morphology between the glass–ceramic sealant and metallic interconnect. The energy dispersive spectrometer (EDS) module attached with the SEM was used for composition analysis to show the elemental distribution in the glass–ceramic sealant and metallic interconnect. Failure modes of the joint under tensile and shear loading were also characterized.

3. Results and discussion

3.1. Effect of number of initial spreading side of glass–ceramic sealant

Comparison of shear strength between the joint specimens with a single side (HT900S) and two sides (HT900D) of glass–ceramic sealant is shown in Fig. 2(a). In Fig. 2(a), the height of a column indicates the average strength and the upper and lower ends of an error bar represent the maximum and minimum strength, respectively. Note that the strength value was calculated by dividing the maximum applied force in each test by the joining area. Therefore, both the shear and the tensile joint strength presented in the current study should be considered as a "nominal" fracture strength. For the single-sided HT900S specimens, the average shear joint strength at room temperature is of 4.9 MPa and decreases to 4.4 MPa at 800 °C. The average shear joint strength of the double-sided HT900D specimens is of 6.6 MPa at room temperature and drops to 4.7 MPa at 800 °C. The shear joint strength in both sealing preparation configurations follows the same decreasing trend with increasing temperature. As shown in Fig. 2(a), shear joint strength is enhanced for the double-sided specimens as compared to the single-sided ones. Fig. 2(b) shows the comparison of tensile strength for the single-sided and double-sided joint specimens. For the HT900S specimens, the average tensile joint strength is reduced from 16.7 MPa at room temperature to 4.3 MPa at 800 °C. The average tensile joint strength of the HT900D specimens drops from

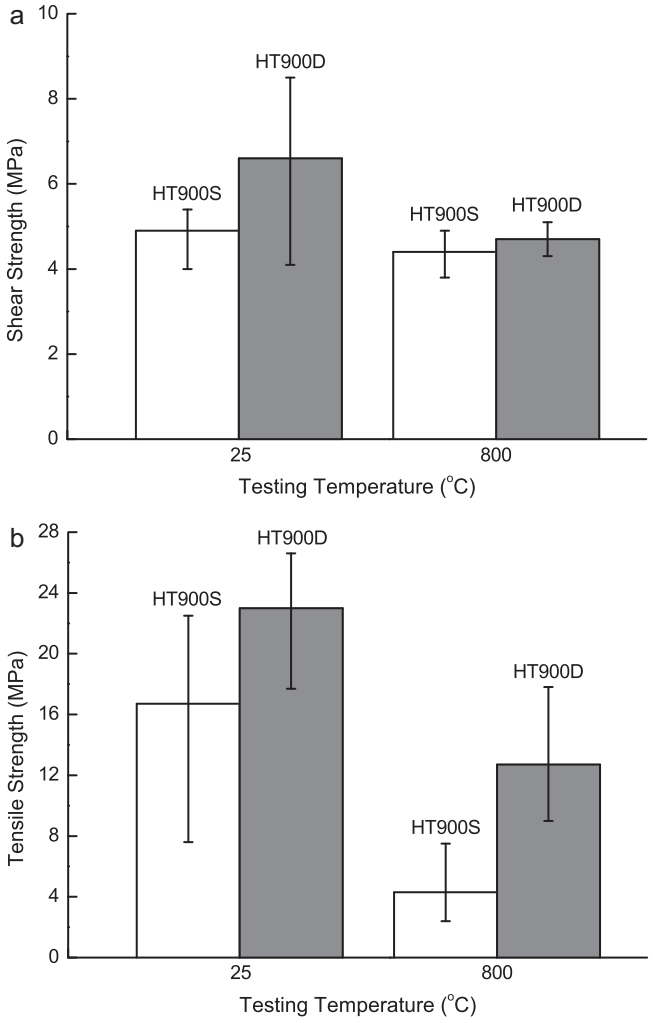

Fig. 2. Comparisons of joint strength for specimens with a single side (HT900S) and two sides (HT900D) of glass–ceramic sealant: (a) shear strength and (b) tensile strength.

23 MPa at room temperature to 12.7 MPa at 800 °C. As shown in Fig. 2(b), tensile joint strength is also enhanced by initially spreading glass–ceramic sealant on each of the two metallic coupons. In particular, an increment of 195% in average tensile joint strength at 800 °C is observed for HT900D as compared to HT900S. The nominal tensile joint strength of HT900S and HT900D is much lower than the flexural strength of the bulk GC-9 glass–ceramic [14] and the tensile strength of the Crofer 22 H alloy [18] at both room temperature and 800 °C. Note the Weibull characteristic flexural strength of a non-aged, sintered GC-9 glass–ceramic is of 42 MPa at room temperature and 19 MPa at 800 °C [14]. The Crofer 22 H alloy has an ultimate tensile strength of 567 MPa at room temperature and 123 MPa at 800 °C [18]. It indicates the fracture modes and strength-determining flaws/defects in the given joints are different from those in the bulk GC-9 glass–ceramic and Crofer 22 H stainless steel. In addition, at a given testing temperature, the tensile joint strength is generally greater than the shear joint strength. This is related to different failure patterns in tensile and shear modes, which will be discussed below.

Representative force–displacement curves for the joint specimens tested in shear mode at room temperature and 800 °C are shown in Fig. 3(a). The force–displacement curve at room temperature exhibits a typical brittle fracture pattern, while that at 800 °C indicates a non-linear failure mode. As the testing temperature of

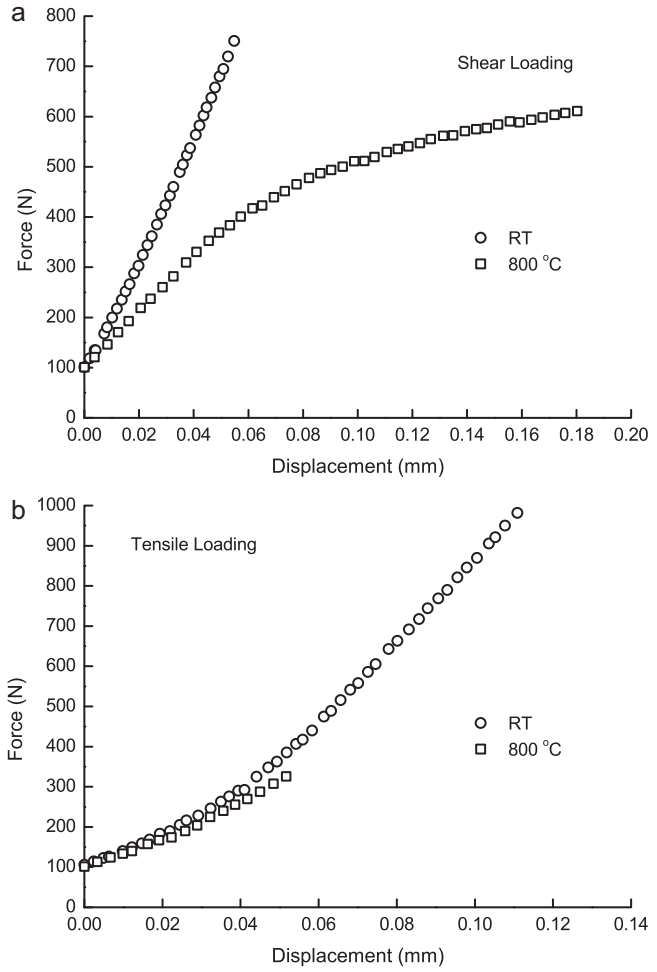

Fig. 3. Typical force–displacement curves of the joint specimens tested under (a) shear and (b) tensile loading at room temperature and 800 °C.

800 °C is higher than the glass transition temperature of the GC-9 glass–ceramic [16], failure of the shear joint specimens at 800 °C becomes a non-linear ductile mode. For the joint specimens tested under tensile loading at room temperature and 800 °C, the typical force–displacement curves are shown in Fig. 3(b). Note the initial non-linear behavior in the force–displacement curves of Fig. 3(b) is due to some compliance of the pin-loading test rigs. In contrast to the shear mode, the force–displacement curves under tensile loading exhibit a brittle fracture pattern at both room temperature and 800 °C. Apparently, the expected high-temperature viscous behavior of the GC-9 glass–ceramic sealant did not influence the tensile force–displacement response at 800 °C. As shown in Fig. 3(b), the fracture force and final displacement in tensile mode are significantly reduced at 800 °C indicating a greater extent of strength decreasing with increasing temperature, in comparison with the shear mode. No significant difference in the load–displacement curves was found between the single-sided and double-sided joint specimens in both shear and tensile modes.

Typical fracture patterns in the single-sided HT900S shear specimens are shown in Fig. 4. Note that fracture surfaces on each half of the broken specimen are presented in Fig. 4 and the following similar figures. As shown in Fig. 4(a), the Crofer 22 H substrate of each fracture surface is still adhered with some GC-9 glass–ceramic sealant. As shown in Fig. 4(a), there are two dark regions, identified as peeled Cr_2O_3 chromia, on top of the glass–ceramic layer in the upper fracture surface, and two counterpart regions with metallic luster of the metal substrate appear in the other fracture

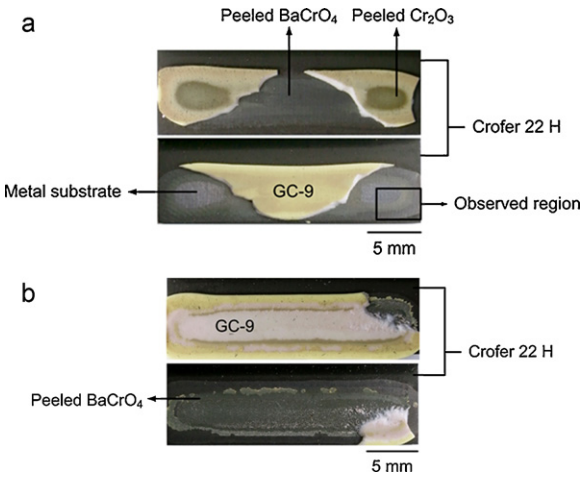

Fig. 4. Failure patterns of HT900S shear specimens tested at (a) room temperature and (b) 800 °C.

surface. The yellow region in the lower fracture surface of Fig. 4(a) is a leftover of the delaminated GC-9 glass–ceramic layer while composition of the counterpart region in the upper fracture surface is identified as a $BaCrO_4$ chromate. Therefore, fracture of the HT900S shear joint specimens at room temperature took place through delamination of the interfaces between the glass–ceramic substrate and $BaCrO_4$ chromate and between the metal substrate and Cr_2O_3 chromia. However, as shown in Fig. 4(b), fracture of the HT900S shear joint specimens at 800 °C occurred through delamination of the interface of GC-9/$BaCrO_4$ (in the peripheral area) as well as within the glass–ceramic layer (in the central white area). The central white region shown in the upper fracture surface of Fig. 4(b) is the interior of the GC-9 glass–ceramic layer. No delamination of the interface of Crofer 22 H/Cr_2O_3 was found in the HT900S shear joint specimens tested at 800 °C.

Identification of each layer shown in Fig. 4 is confirmed through SEM/EDS analysis. Fig. 5(a) shows an SEM micrograph of the observed region outlined in the lower fracture surface of Fig. 4(a). There are three distinct zones with variously gray levels in this observed region. As shown in Fig. 5(a), the three zones, outlined by the dash lines, are the metal substrate, $BaCrO_4$ chromate layer, and Cr_2O_3 chromia layer. By means of EDS analysis, element distributions in these three zones were obtained and shown in Fig. 5(b)–(f). As shown in Fig. 5(b), a high intensity of Fe is found in the metal substrate zone. The mappings of Cr, Mn, and O shown in Fig. 5(c)–(e) agree with the corresponding zones. The shape of the region with a high intensity of Ba in Fig. 5(f) agrees with that supposed to be a peeled $BaCrO_4$ layer. These evidences indicate that fracture of the shear joint specimens indeed involves delamination of the glass–ceramic substrate/chromate and metal substrate/chromia interfaces. High-magnification SEM micrographs of the three zones in Fig. 5(a) are shown in Fig. 6. A smooth surface is observed at the metal substrate zone (Fig. 6(a)) while a rough surface is found for the peeled $BaCrO_4$ zone (Fig. 6(b)). A crystal structure is visible at the chromia oxide zone, as shown in Fig. 6(c). Such crystals are the $(Cr,Mn)_3O_4$ spinels on top of the Cr_2O_3 chromia.

Fracture patterns of the double-sided HT900D shear specimens are similar to those of single-sided ones (HT900S) at each given testing temperature. That is, fracture of the HT900D shear specimens took place through delamination of the GC-9/$BaCrO_4$ and Crofer 22 H/Cr_2O_3 interfaces at room temperature and at the interface of GC-9/$BaCrO_4$ as well as in the GC-9 layer at 800 °C.

Fig. 7 shows the typical fracture patterns in single-sided HT900S tensile specimens tested at room temperature and 800 °C. As shown in Fig. 7(a), fracture occurred mostly within the glass–ceramic

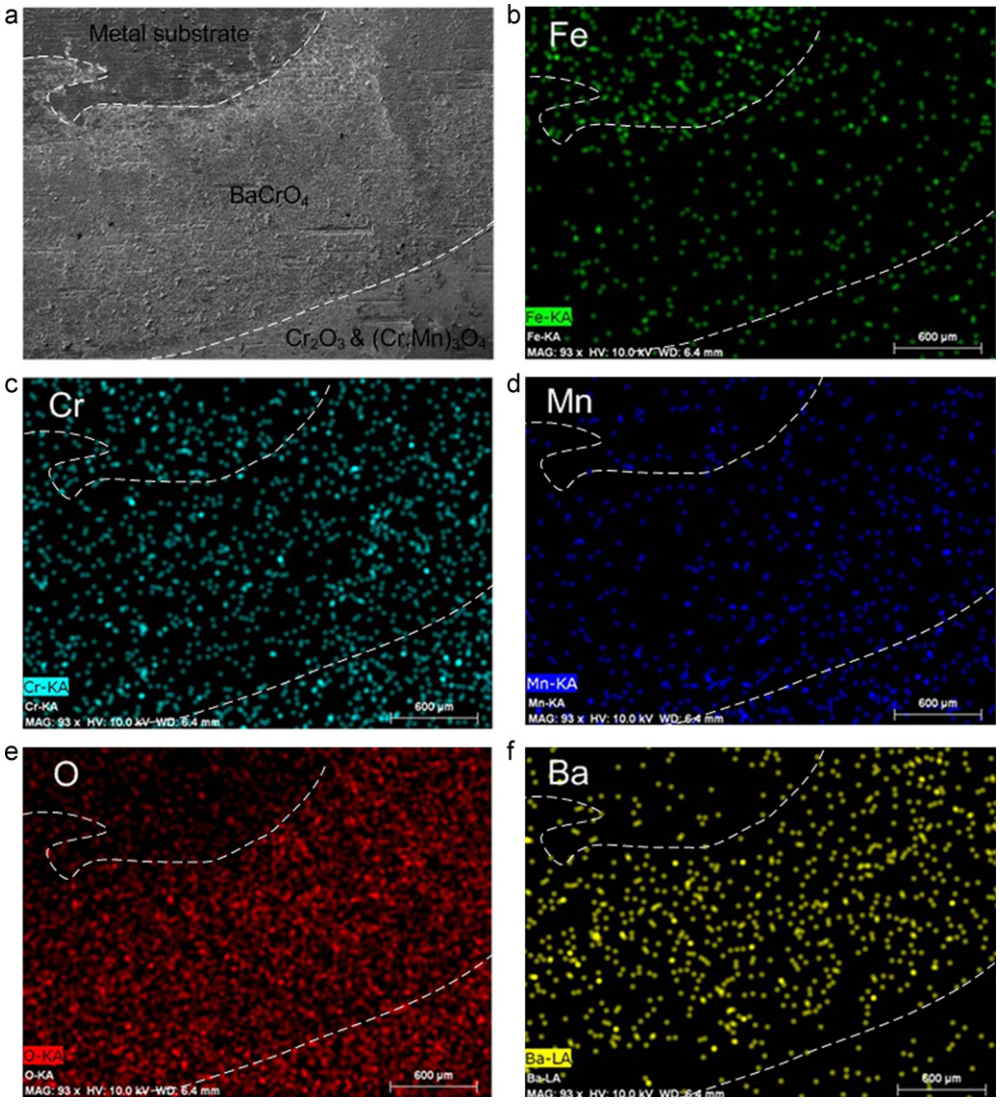

Fig. 5. EDS mapping of elements on the fracture surface outlined in Fig. 4(a): (a) observed region; (b) Fe; (c) Cr; (d) Mn; (e) O; and (f) Ba.

layer. However, for the HT900S tensile specimens tested at 800 °C, fracture also occurred in the glass–ceramic layer, while delamination was occasionally observed at the interface of GC-9/$BaCrO_4$ (Fig. 7(b)). For the double-sided HT900D tensile specimens, fracture took place mainly in the glass–ceramic layer at both room temperature and 800 °C. These results indicate that the tensile joint strength accompanied by fracture of the glass–ceramic layer alone is higher than that with fracture of both glass–ceramic layer and interface of GC-9/$BaCrO_4$.

In the present study, a half specimen was made by spreading the GC-9 slurry on the surface of a Crofer 22 H coupon. The half specimen was then put into a furnace at 70 °C to dry the paste. During the joining process at high temperatures, the half specimen was placed on another half specimen or a plain metal coupon to make a double-sided or single-sided specimen, respectively. For a single-sided specimen, no glass was initially spread on the plain metal coupon to be joined. However, for a double-sided specimen, glass has been spread on each of the two metal coupons before the joining process. The wettability of the glass slurry initially spread on the metal slice at room temperature is better than that of the dry glass–ceramic in direct contact with the metal slice during joining at high temperatures. A good wetting behavior of glass on the metal surface can improve the bonding performance. In this regard, the superiority of joint strength in double-sided specimens over that in single-sided ones is attributed to a better wetting effect during joining at high temperatures. Fractography analyses of the single-sided shear specimens indicate fracture all occurred at the interfaces of the side without glass initially. This is an evidence of a weaker bonding performance in the single-sided specimen.

3.2. *Effect of pre-oxidation of metallic interconnect*

An oxide layer on metal is favorable for bonding a glass with metal as the oxide layer during sealing process can dissolve into the glass to promote the wetting behavior of glass to metal [26]. As described above, the results in Refs. [10,11] show a different trend regarding the effect of pre-oxidation of metallic interconnect. In this regard, the present study also investigates the pre-oxidation effect on the joint strength by heat treating the Crofer 22 H coupons at 900 °C in air for 2 h (designated as POHT900D) or 20 h (designated as LPOHT900D) before joining with the GC-9 glass–ceramic. Comparisons of joint strength for the cases with and without pre-oxidation of Crofer 22 H coupons are shown in Fig. 8. As shown in Fig. 8(a), the average shear joint strength of HT900D at room temperature is of 6.6 MPa and decreases to 4.7 MPa at 800 °C. For the pre-oxidized POHT900D specimens, the average shear joint

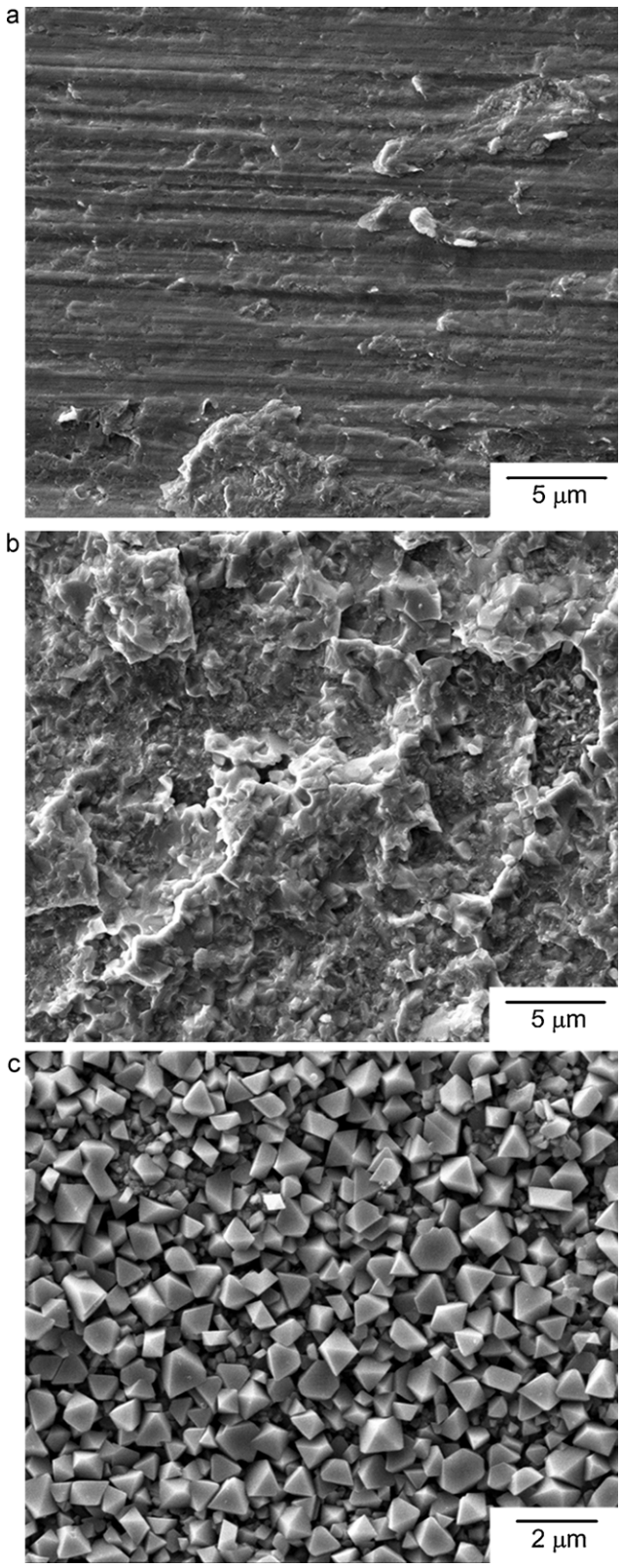

Fig. 6. High-magnification SEM micrographs of the three zones shown in Fig. 5: (a) metal substrate; (b) $BaCrO_4$ chromate; and (c) $(Cr,Mn)_3O_4$ spinels.

strength at room temperature is of 7 MPa and drops to 4.4 MPa at 800 °C. As shown in Fig. 8(b), the average tensile joint strength at room temperature is decreased from 23 MPa of HT900D to 16.7 MPa of POHT900D due to a 2-h pre-oxidation treatment while the counterparts at 800 °C are comparable. Apparently, a 900 °C/2 h

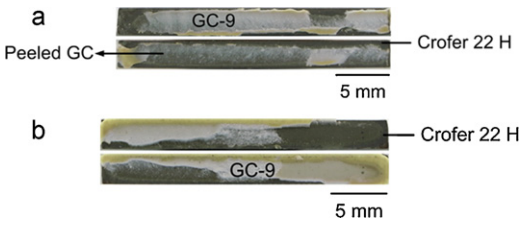

Fig. 7. Failure patterns of HT900S tensile specimens tested at (a) room temperature and (b) 800 °C.

pre-oxidation treatment of the metallic interconnect does not significantly improve the shear or tensile joint strength for the given Crofer 22 H/GC-9/Crofer 22 H joints.

The tensile joint strength at 800 °C for variously pre-oxidized times is shown in Fig. 9. The average tensile joint strength of HT900D at 800 °C is of 12.7 MPa and comparable with that (12.6 MPa) of the 2-h pre-oxidized POHT900D. However, for the 20-h pre-oxidized LPOHT900D specimens, the average tensile joint strength is of 7 MPa. The tensile joint strength for a 900 °C/20 h pre-oxidation treatment is considerably degraded indicating that a long-term pre-oxidation treatment of the Crofer 22 H coupons deteriorates the bonding performance between the GC-9 glass ceramic and Crofer 22 H alloy. Both the shear and the tensile joint

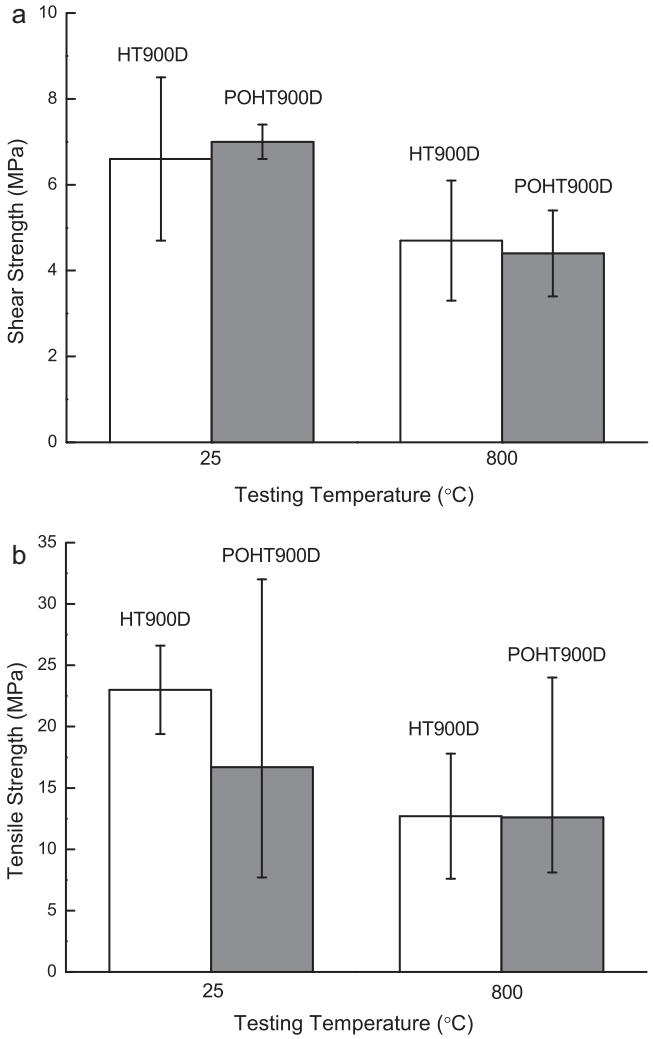

Fig. 8. Comparisons of joint strength of specimens with and without pre-oxidation of metal coupons: (a) shear strength and (b) tensile strength.

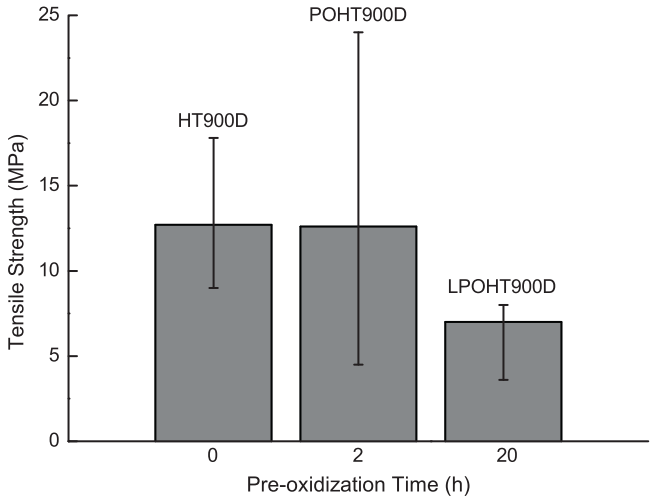

Fig. 9. Tensile joint strength at 800 °C for specimens with various pre-oxidation treatment times.

strength results shown in Figs. 8 and 9 clearly indicate that neither a 900 °C/2 h nor a 900 °C/20 h pre-oxidation treatment of the given metallic interconnect could effectively improve the bonding strength between the given glass–ceramic sealant and metallic interconnect.

Fractography analyses indicate that failure patterns for the pre-oxidized POHT900D shear specimens are similar to those of HT900D ones. This might explain why the shear joint strength is not enhanced by the given 2-h pre-oxidation treatment. As shown in Fig. 10, most of the fracture in the pre-oxidized POHT900D tensile specimens took place in the glass–ceramic layer at both room temperature and 800 °C, while delamination is occasionally observed at the interface of GC-9/$BaCrO_4$. Note that fracture of the tensile joint specimens without pre-oxidation (HT900D) all took place within the glass–ceramic layer. For the 20-h pre-oxidized tensile specimens (LPOHT900D) tested at 800 °C, extensive delamination of the GC-9/$BaCrO_4$ interface is observed on the fracture surface in comparison with the 2-h pre-oxidized ones. Such a greater extent of delamination failure might explain why the tensile joint strength is significantly reduced by a long-term pre-oxidation treatment of the Crofer 22 H coupons.

Fig. 11(a) shows a cross-sectional SEM micrograph of the interface between the GC-9 glass–ceramic and Crofer 22 H alloy in an HT900D joint specimen without pre-oxidation. Two distinct zones are observed in Fig. 11(a) with the upper zone representing the GC-9 glass–ceramic sealant and the lower region representing the Crofer 22 H. A good adhesion between the glass–ceramic

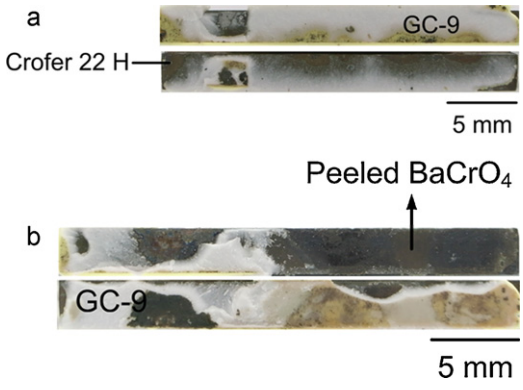

Fig. 10. Failure patterns of tensile joint specimens of POHT900D tested at (a) room temperature and (b) 800 °C.

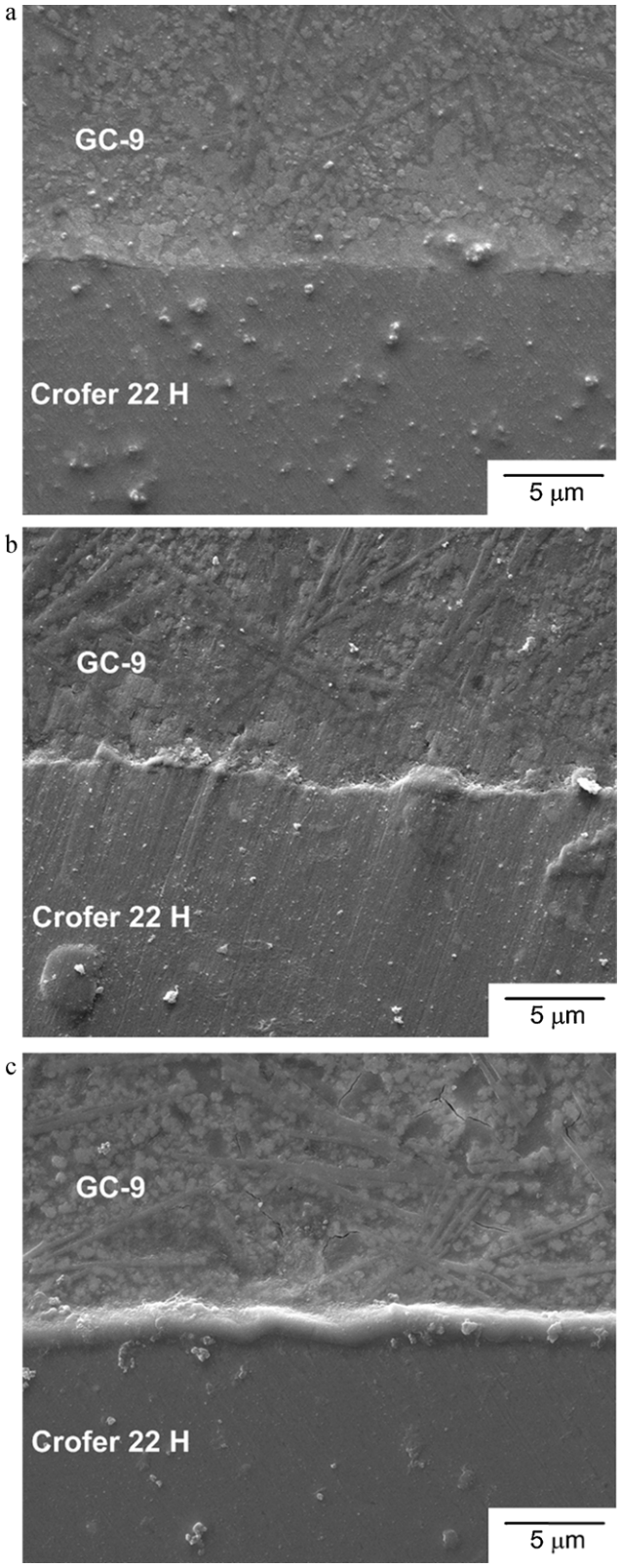

Fig. 11. Cross-sectional SEM micrographs of the interface between the GC-9 and Crofer 22 H in plain and variously pre-oxidized joint specimens: (a) HT900D; (b) POHT900D; and (c) LPOHT900D.

sealant and metallic interconnect is observed. A continuous and defect/crack-free interface is present indicating a good physical compatibility between the two materials. The Cr_2O_3 chromia layer on the metal side of HT900D is too thin to be observed.

A cross-sectional SEM micrograph of the interface in POHT900D is shown in Fig. 11(b). For the 2-h pre-oxidized POHT900D specimen, a good adhesion is also observed and a bright, non-uniform chromia layer on the metal side is visible at the interface (Fig. 11(b)). The thickness of the Cr_2O_3 chromia layer in POHT900D is about 0.3 μm. Fig. 11(c) shows the SEM micrograph of a cross-section of the interface of GC-9/Crofer 22 H in a LPOHT900D specimen with a 20-h pre-oxidation treatment. As shown in Fig. 11(c), a good adhesion between the glass–ceramic sealant and metallic interconnect is also observed. As compared to Fig. 11(a) and (b), the chromia oxide layer in LPOHT900D is thicker and more uniform. The thickness of the Cr_2O_3 layer in LPOHT900D is about 1.1 μm (Fig. 11(c)). In corresponding to the mechanical testing results presented in Fig. 9, the microstructural observations indicate that the joint strength is significantly degraded if the thickness of the chromia layer is greater than 1 μm. Such a trend is also reported in Ref. [11] but different from that in Ref. [10]. The tensile joint strength of a YSO75 glass with Crofer 22 APU is degraded if the thickness of oxide scale on Crofer 22 APU is greater than 1–2 μm [11]. However, oxide scales thinner than 0.5 μm do not influence the tensile joint strength of YSO75/Crofer 22 APU [11]. Although Ref. [10] reported that a pre-oxidation treatment of AISI 430 steel could generate a 1–2-μm thick chromium–manganese–iron oxide layer and improve the bonding performance between an SACN glass and AISI 430 steel, the conclusions were made based on microstructural observations without mechanical testing of joint strength. A microstructurally good adhesion between the glass–ceramic sealant and metallic interconnect is still present in both short- and long-term pre-oxidized joint specimens (POHT900D and LPOHT900D) in the current study, but the given pre-oxidation treatments do not generate any beneficial effect on the joint strength according to the mechanical testing results.

3.3. Effect of thermal aging

As some of the joints in pSOFCs are exposed to an oxidizing environment during operation, it is important to characterize the aging effect on the joint strength at elevated temperature. In this study, some of the joined specimens were aged in air at 800 °C for 250 h, 500 h, and 1000 h (designated as HT900D-A250, HT900D-A500, and HT900D-A1000, respectively) to assess the effect of thermal aging on the mechanical strength of joint. The aged joint specimens were tested under shear loading at 800 °C. Comparison of shear strength for the unaged and aged joint specimens is given in Fig. 12. For the HT900D-A250 and HT900D-A500 specimens, the average shear strength at 800 °C is of 3.9 MPa. For the HT900D-A1000 specimens, the average shear strength is slightly decreased to 3.8 MPa. In general, the shear strength of the joint specimens aged to different degrees is comparable. Compared to the shear strength (4.7 MPa) of the unaged, as-sealed joint specimens, a reduction of 17–19% in strength is observed for the aged ones. However, increasing the aging time from 250 h to 500 h and even to 1000 h does not further degrade the joint strength to a significantly greater extent.

Fig. 13 shows the typical fracture patterns of the aged specimens tested under shear loading at 800 °C. In Fig. 13(a), the fracture pattern of HT900D-A250 shows delamination of the GC-9/$BaCrO_4$ interface is the primary failure mode. A similar fracture pattern is observed for the HT900D-A500 specimens. For HT900D-A1000, in addition to delamination of the GC-9/$BaCrO_4$ interface at the outer rim, fracture mainly occurred within the glass–ceramic layer and color of the glass–ceramic layer turned into brown from white (Fig. 13(b)). Although the fracture pattern is changed for a longer aging time (1000 h), the joint strength is comparable with that of a shorter aging time (250 h and 500 h).

It has been reported that a greater flexural strength and stiffness at 700–800 °C is observed for a 100-h or 1000-h thermally aged, sintered GC-9 glass over a non-aged one due to a greater extent of crystallization [14,27]. Flexural strength of the thermally aged GC-9 glass–ceramic is increased with an increase in aging time from 100 h to 1000 h [27]. Crystallization of glass sealant is expected to take place in the thermally aged joint specimens (HT900D-A250, -A500, and -A1000), too. However, the shear strength of the thermally aged joint specimens does not increase with thermal aging time but shows an opposite trend in the present study. It indicates that the shear joint strength is dominated by the interfacial properties rather than by the strength of bulk glass–ceramic. During the joining process at high temperatures, $BaCrO_4$ chromate is formed on the surface of the glass–ceramic sealant. Due to the high CTE and anisotropy of chromate, high thermal stresses are expected to generate cracks in the joint specimens during cooling from high temperature [11]. After a thermal aging treatment in air, the amount of chromate in a joint specimen becomes greater, as compared to the unaged one. The strength degradation of aged joint specimens in the present study is thus attributed to an extensive growth of $BaCrO_4$ chromate layer. For HT900D-A250 and HT900D-A500 specimens, fracture thus occurred mainly at the interface

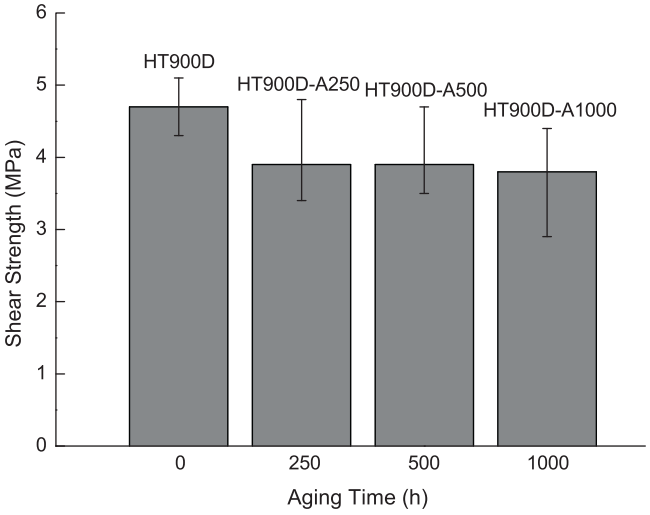

Fig. 12. Shear joint strength at 800 °C for specimens with variously thermal aging times.

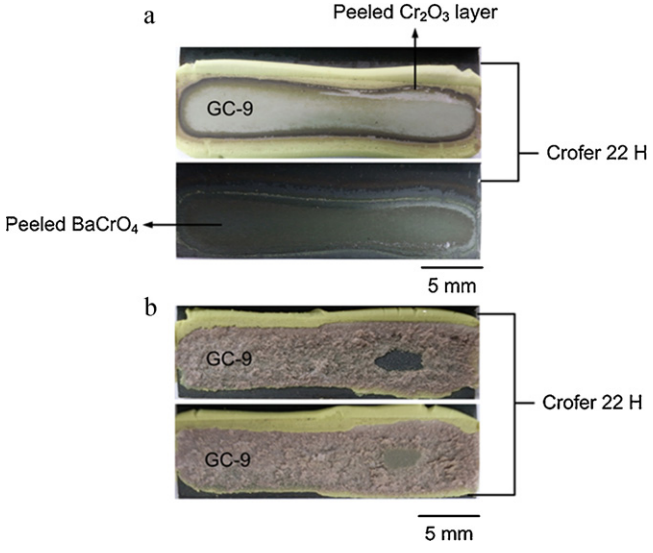

Fig. 13. Failure patterns of variously aged shear specimens tested at 800 °C: (a) HT900D-A250 and (b) HT900D-A1000.

between the $BaCrO_4$ chromate and the glass–ceramic substrate and the chromate was uniformly peeled off, as shown in Fig. 13(a).

A greater extent of crystallization of glass sealant is expected to take place in the 1000-h aged joint specimens (HT900D-A1000). However, in the study of Liu et al. [28], micro-voids due to CTE difference between the ceramic and glass phases are formed in the glass–ceramic sealant during a cooling process. For HT900D-A1000 specimens, fracture mainly took place in the glass–ceramic layer resulting from growth of micro-voids. Typical SEM micrographs of fracture surface on the glass–ceramic layer in the HT900D, HT900D-A500, and HT900D-A1000 shear specimens are shown in Fig. 14. As shown in Fig. 14(a), on the fractured glass–ceramic layer in the unaged HT900D specimen, needle-shape crystals and aggregated particles are observed and interfacial delamination is along these needle-shape crystals. As shown in Fig. 14(b) for HT900D-A500, needle-shape crystals and aggregated particles are also observed and the amount of aggregated particles is greater than that in HT900D. As shown in Fig. 14(c), the amount of aggregated particles in HT900D-A1000 is much larger than that in HT900D and HT900D-A500. As fracture of the HT900D-A1000 specimens mostly took place within the glass–ceramic layer, needle-shape crystals are barely observed on the fracture face (Fig. 14(c)). In addition, a considerable amount of micro-voids are found between the aggregated particles and glass phase in HT900D-A1000. These micro-voids are presumably responsible for the fracture in the glass–ceramic layer. Although fracture of the HT900D-A1000 specimens mostly took place within the glass–ceramic layer and involved micro-voids, it still initiated from the GC-9/$BaCrO_4$ interface at the outer rim (Fig. 13(b)). This might explain why the shear joint strength of HT900D-A1000 is comparable with that of HT900D-A250 and -A500.

A cross-sectional SEM micrograph of the interface between the GC-9 and Crofer 22 H in a 1000 h-aged joint specimen is shown in Fig. 15. A good physical compatibility between the glass–ceramic and metallic interconnect is observed at the interface where no defects or cracks are found. As shown in Fig 15, both the Cr_2O_3 chromia layer from the metal side and the $BaCrO_4$ chromate layer from the glass–ceramic side can be clearly seen in such a long-term aged joint specimen. The chromia oxide layer in the HT900D-A1000 specimen (Fig. 15) has a thickness of about 0.4 μm which is larger than that in the unaged HT900D specimen (Fig. 11(a)). Above the chromia layer shown in Fig. 15, a rough and light-gray $BaCrO_4$ chromate layer is found. EDS analysis of this layer indicates that it contains a substantial amount of Ba, Cr, and O and confirms that it is the $BaCrO_4$ chromate with a thickness of about 1.5 μm. Such a $BaCrO_4$ chromate layer is too thin to be measured in the unaged HT900D specimen (Fig. 11(a)). The SEM micrograph shown in Fig. 15 confirms that thickness of the $BaCrO_4$ chromate layer in the joint specimen is increased with aging time at 800 °C.

3.4. Overall comparison

An overall comparison of the joint strength and fracture mode for all the given testing conditions is given in Tables 1 and 2. Table 1 lists the average shear joint strength and fracture site for all the tested shear specimens. As described above, three types of fracture site are observed in the shear joint specimens. Fracture in the GC-9 glass–ceramic layer is designated as "A". Fracture at the interface of GC-9/$BaCrO_4$ is designated as "B" while fracture at the interface of Crofer 22 H/Cr_2O_3 is designated as "C". If fracture involves two sites, these two fracture sites are marked together. For all the shear specimens tested at room temperature, B and C are the primary fracture sites while HT900S accompanied by a greater delamination area at B has the lowest shear joint strength. For all the shear specimens tested at 800 °C except the long-term aged HT900D-A1000, the joint strength of specimens with A + B fracture sites is greater than that of specimens with B only. Apparently, the interface between the GC-9 glass–ceramic substrate and $BaCrO_4$ chromate layer is the weakest layer to resist a shear loading for the joint specimens.

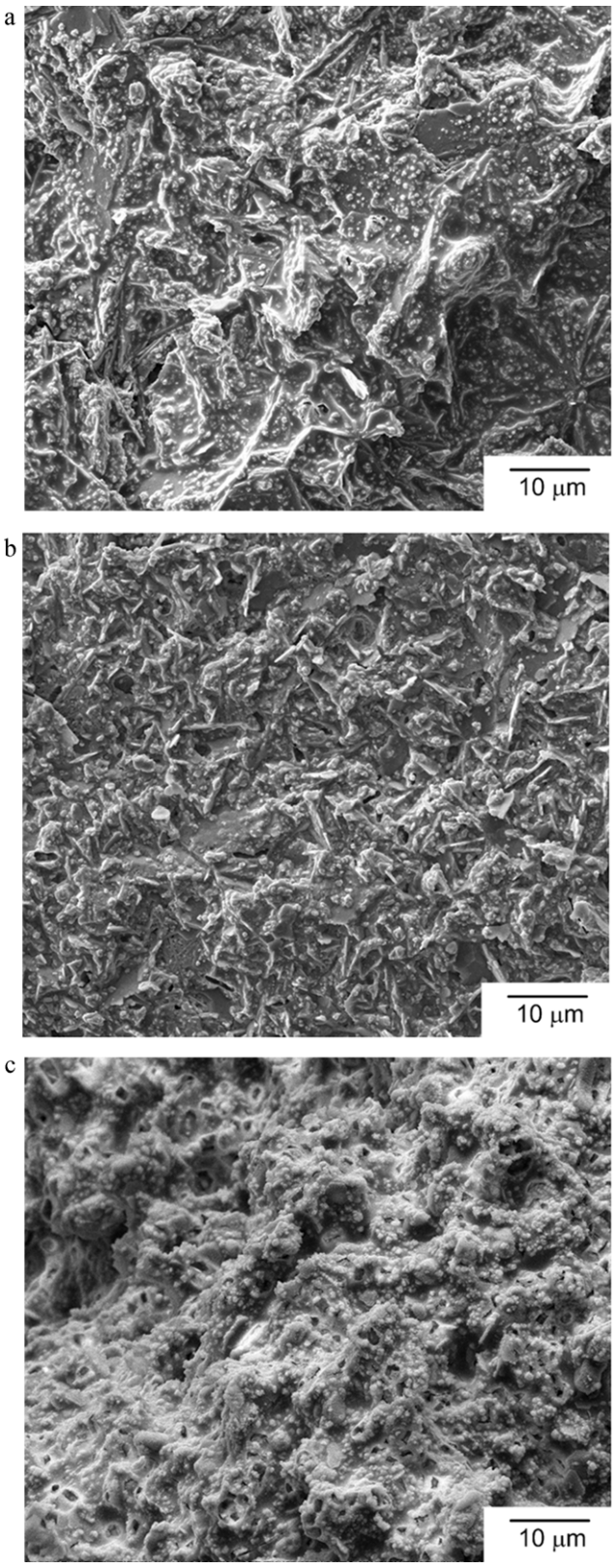

Fig. 14. SEM micrographs of fracture surface on the glass–ceramic layer in the shear specimens tested at 800 °C: (a) unaged HT900D; (b) aged HT900D-A500; and (c) aged HT900D-A1000.

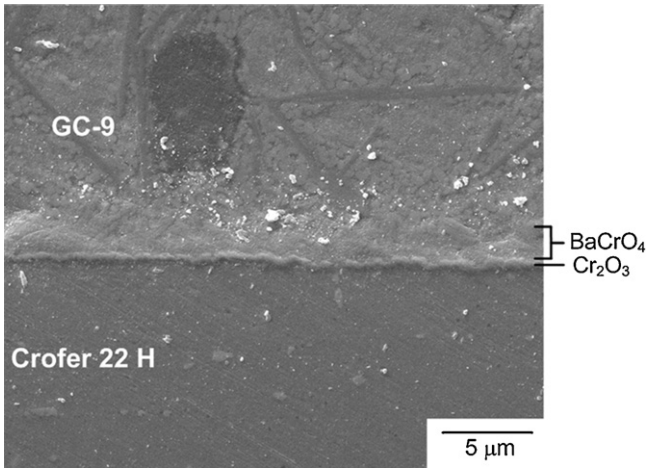

Fig. 15. Cross-sectional SEM micrograph of the interface between the GC-9 and Crofer 22 H in an aged HT900D-A1000 joint specimen.

Table 1
Shear joint strength and fracture site of tested joint specimens.

Test temperature (°C)	Specimen condition	Average shear strength (MPa)	Fracture site[a]
25	HT900S	4.9	B + C
25	HT900D	6.6	B + C
25	POHT900D	7.0	B + C
800	HT900S	4.4	A + B
800	HT900D	4.7	A + B
800	POHT900D	4.4	A + B
800	HT900D-A250	3.9	B
800	HT900D-A500	3.9	B
800	HT900D-A1000	3.8	A + B

[a] A: in glass–ceramic sealant layer; B: at the interface between glass–ceramic substrate and $BaCrO_4$ layer; C: at the interface between metal substrate and Cr_2O_3 layer.

Table 2 lists the average tensile joint strength and fracture site for all the tested tensile joint specimens. Fracture sites A and B are mostly observed for the tensile joint specimens while fracture at the interface of Crofer 22 H/Cr_2O_3 (site C) is not observed. Given a test temperature, the tensile joint strength of specimens with A + B fracture sites is less than that of those with A only. It indicates that the tensile joint strength is lower if fracture involves delamination at the interface between the GC-9 glass–ceramic substrate and $BaCrO_4$ chromate layer. Again, the interface of GC-9/$BaCrO_4$ is the weakest layer in the joint specimen to resist tensile loading like that in the shear mode. A similar result was also found in Ref. [13]. As reported in Ref. [13], for the joint specimens of a G-18 glass with Crofer 22 APU alloy tested under tensile loading, an interfacial fracture mode accompanied a lower joining strength in comparison with the case of fracture taking place within the bulk glass sealant.

Results in the present study and Ref. [11] both indicate that formation of chromate along the Cr-containing metallic interconnects and silicate glass/glass–ceramic sealants containing alkaline earths such as Ba and/or Sr leads to a lower joint strength in the pre-oxidized as well as thermally aged joint specimens. Therefore, how to lessen formation of chromate to enhance both the shear and the tensile joint strength between glass/glass–ceramic sealant and metallic interconnect is an important issue for future development of pSOFC glass/glass–ceramic sealants.

Table 2
Tensile joint strength and fracture site of tested joint specimens.

Test temperature (°C)	Specimen condition	Average tensile strength (MPa)	Fracture site
25	HT900S	16.7	A
25	HT900D	23.0	A
25	POHT900D	16.7	A + B
800	HT900S	4.3	A + B
800	HT900D	12.7	A
800	POHT900D	12.6	A + B
800	LPOHT900D	7.0	A + B

4. Conclusions

(1) A technique of measuring the shear and tensile joint strength between glass/glass–ceramic sealant and metallic interconnect at room temperature and 800 °C is developed in the present study. The joint strength of Crofer 22 H/GC-9/Crofer 22 H sandwich specimens initially with two sides of glass–ceramic sealant is greater than that of single-sided ones. In particular, an increment of 195% in tensile joint strength at 800 °C is found for the double-sided specimens, as compared to the single-sided ones.
(2) A pre-oxidation treatment of Crofer 22 H coupons at 900 °C for 2 h does not improve the shear or tensile joint strength for all the given testing conditions. In particular, a longer pre-oxidation time of 20 h even considerably reduces the tensile joint strength at 800 °C by an extent of 45%.
(3) A thermal aging in air at 800 °C for 250 h or 500 h degrades the shear joint strength at 800 °C by 17% due to continuous growth of $BaCrO_4$ chromate over time. A longer aging time of 1000 h reduces the shear joint strength by a slightly additional extent from 17% to 19%.
(4) The interface between the GC-9 glass–ceramic substrate and $BaCrO_4$ chromate layer is generally the weakest layer to resist a shear loading for the joint specimens. For shear joint specimens with a 1000-h thermal aging treatment in air, fracture mainly occurs in the GC-9 layer resulting from growth of micro-voids within the glass–ceramic layer.
(5) For the tensile joint specimens, a greater joint strength corresponds to fracture occurring only in the glass–ceramic sealant layer. For a lower tensile joint strength, delamination at the interface between the GC-9 substrate and $BaCrO_4$ layer is also involved in the fracture in addition to the fracture of glass–ceramic layer.

Acknowledgement

This work was supported by the Institute of Nuclear Energy Research under Contract Nos.: 99-2001-INER-047 and 100-2001-INER-053.

References

[1] C.-K. Lin, T.-T. Chen, Y.-P. Chyou, L.-K. Chiang, J. Power Sources 164 (2007) 238–251.
[2] C.-K. Lin, L.-H. Huang, L.-K. Chiang, Y.-P. Chyou, J. Power Sources 192 (2009) 515–524.
[3] F. Smeacetto, M. Salvo, P. Leone, M. Santarelli, M. Ferraris, Mater. Lett. 65 (2011) 1048–1052.
[4] A. Goel, D.U. Tulyaganov, V.V. Kharton, A.A. Yaremchenko, J.M.F. Ferreira, J. Power Sources 195 (2010) 522–526.
[5] F. Smeacetto, A. Chrysanthou, M. Salvo, Z. Zhang, M. Ferraris, J. Power Sources 190 (2009) 402–407.
[6] F. Smeacetto, M. Salvo, M. Ferraris, J. Cho, A.R. Boccaccini, J. Eur. Ceram. Soc. 28 (2008) 61–68.
[7] P. Batfalsky, V.A.C. Haanappel, J. Malzbender, N.H. Menzler, V. Shemet, I.C. Vinke, R.W. Steinbrech, J. Power Sources 155 (2006) 128–137.
[8] N.H. Menzler, D. Sebold, M. Zahid, S.M. Gross, T. Koppitz, J. Power Sources 152 (2005) 156–167.
[9] V.A.C. Haanappel, V. Shemet, S.M. Gross, T. Koppitz, N.H. Menzler, M. Zahid, W.J. Quadakkers, J. Power Sources 150 (2005) 86–100.
[10] F. Smeacetto, M. Salvo, M. Ferraris, V. Casalegno, P. Asinari, A. Chrysanthou, J. Eur. Ceram. Soc. 28 (2008) 2521–2527.
[11] Y.-S. Chou, J.W. Stevenson, P. Singh, J. Power Sources 184 (2008) 238–244.
[12] Y.-S. Chou, J.W. Stevenson, P. Singh, J. Power Sources 185 (2008) 1001–1008.

[13] E.V. Stephens, J.S. Vetrano, B.J. Koeppel, Y. Chou, X. Sun, M.A. Khaleel, J. Power Sources 193 (2009) 625–631.
[14] H.-T. Chang, C.-K. Lin, C.-K. Liu, S.-H. Wu, J. Power Sources 196 (2011) 3583–3591.
[15] H.-T. Chang, C.-K. Lin, C.-K. Liu, J. Power Sources 195 (2010) 3159–3165.
[16] H.-T. Chang, C.-K. Lin, C.-K. Liu, J. Power Sources 189 (2009) 1093–1099.
[17] Y.-T. Chiu, C.-K. Lin, J.-C. Wu, J. Power Sources 196 (2011) 2005–2012.
[18] Y.-T. Chiu, C.-K. Lin, J. Power Sources 198 (2012) 149–157.
[19] C.-K. Liu, T.-Y. Yung, K.-F. Lin, Proceedings of the Annual Conference of the Chinese Ceramic Society 2007 (CD-ROM), 2007 (in Chinese).
[20] C.-K. Liu, T.-Y. Yung, S.-H. Wu, K.-F. Lin, Proceedings of the MRS_Taiwan Annual Meeting 2007 (CD-ROM), 2007 (in Chinese).
[21] C.-K. Liu, T.-Y. Yung, K.-F. Lin, Proceedings of the Annual Conference of the Chinese Ceramic Society 2008 (CD-ROM), 2008 (in Chinese).
[22] C.-K. Liu, K.-C. Tsai, K.-F. Lin, S.-H. Wu, T.-Y. Yung, Proceedings of the Annual Conference of the Chinese Ceramic Society 2009 (CD-ROM), 2009 (in Chinese).
[23] C.-K. Liu, T.-Y. Yung, K.-F. Lin, R.-Y. Lee, S.-H. Wu, ECS Trans. 25 (2009) 1491–1500.
[24] J. Froitzheim, G.H. Meier, L. Niewolak, P.J. Ennis, H. Hattendorf, L. Singheiser, W.J. Quadakkers, J. Power Sources 178 (2008) 163–173.
[25] L. Paul, H. Hattendorf, L. Niewolak, B. Kuhn, O. Ibas, W.J. Quadakkers, Proceedings of Fuel Cell Seminar 2010, San Antonio, TX, USA, October, 2010.
[26] I.W. Donald, J. Mater. Sci. 28 (1993) 2841–2886.
[27] J.-H. Yeh, C.-K. Lin, L.-K. Chiang, C.-K. Liu, Proceedings of the 28th Annual Conference of the Chinese Society of Mechanical Engineers (Taiwan), Taichung, Taiwan, December 10–11, 2011.
[28] W. Liu, X. Sun, M.A. Khaleel, J. Power Sources 185 (2008) 1193–1200.